A physical mechanism to explain the delivery of chemical penetration enhancers into skin during transdermal sonophoresis — Insight into the observed synergism

Published in final edited form as:
J Control Release. 2012 March 10; 158(2): 250–260. doi:10.1016/j.jconrel.2011.11.008.

A Physical Mechanism to Explain the Delivery of Chemical Penetration Enhancers into Skin during Transdermal Sonophoresis - Insight into the Observed Synergism

Baris E. Polat, **William M. Deen**, **Robert Langer**[*], and **Daniel Blankschtein**[*]
Department of Chemical Engineering, Massachusetts Institute of Technology, Cambridge, MA 02139, USA

Abstract

The synergism between low-frequency sonophoresis (LFS) and chemical penetration enhancers (CPEs), especially surfactants, in transdermal enhancement has been investigated extensively since this phenomenon was first observed over a decade ago. In spite of the identifying that the origin of this synergism is the increased penetration and subsequent dispersion of CPEs in the skin in response to LFS treatment, to date, no mechanism has been directly proposed to explain *how* LFS induces the observed increased transport of CPEs. In this study, we propose a plausible physical mechanism by which the transport of *all* CPEs is expected to have significantly increased flux into the localized-transport regions (LTRs) of LFS-treated skin. Specifically, the collapse of acoustic cavitation microjets within LTRs induces a convective flux. In addition, because amphiphilic molecules preferentially adsorb onto the gas/water interface of cavitation bubbles, amphiphiles have an additional adsorptive flux. In this sense, the cavitation bubbles effectively act as carriers for amphiphilic molecules, delivering surfactants directly into the skin when they collapse at the skin surface as cavitation microjets. The flux equations derived for CPE delivery into the LTRs and non-LTRs during LFS treatment, compared to that for untreated skin, explain why the transport of all CPEs, and to an even greater extent amphiphilic CPEs, is increased during LFS treatment. The flux model is tested with a non-amphiphilic CPE (propylene glycol) and both nonionic and ionic amphiphilic CPEs (octyl glucoside and sodium lauryl sulfate, respectively), by measuring the flux of each CPE into untreated skin and the LTRs and non-LTRs of LFS-treated skin. The resulting data shows very good agreement with the proposed flux model.

Keywords

Chemical Penetration Enhancers; Diffusion; Sonophoresis; Synergism; Transdermal; Ultrasound

[*]Corresponding authors: Professor Daniel Blankschtein, Department of Chemical Engineering, Room 66-444, Massachusetts Institute of Technology, 77 Massachusetts Avenue, Cambridge, MA 02139, USA, Tel: +1 617 253 4594, Fax: +1 617 252 1651, dblank@mit.edu. Professor Robert Langer, Department of Chemical Engineering, David H. Koch Center for Integrative Cancer Research, Room 76-661, Massachusetts Institute of Technology, 77 Massachusetts Avenue, Cambridge, MA 02139, USA, Tel: +1 617 253 3107, Fax: +1 617 258 8827, rlanger@mit.edu.

1. INTRODUCTION

The use of low-frequency sonophoresis (LFS) for the transdermal delivery of drugs has been shown to be a feasible and emerging method of local, regional, and systemic drug delivery, which allows for the minimization of side effects associated with oral and intravenous delivery.[1, 2] When combined with chemical penetration enhancers (CPEs), such as the surfactant sodium lauryl sulfate (SLS), LFS treatment has been shown to result in a synergistic effect in skin permeability enhancement. [3, 4] This synergism has been primarily studied experimentally, demonstrating that combined treatment with LFS and CPEs (primarily surfactants) allows for decreased treatment times, decreased energy-input requirements, increased skin permeability, higher-connectivity of lacunar regions in the stratum corneum, and less physical skin perturbation compared to the LFS treatment alone. [3–6] The driving force of this synergism is the ability of LFS to not only increase the penetration of CPEs into the skin, but also to deliver CPEs deeply into the skin, including increasing their dispersion in the skin.[3] In the absence of LFS, CPEs are generally limited by their passive diffusion into the skin, owing to the innate barrier properties of the outermost layer of the skin, the stratum corneum. On the other hand, when LFS assists the delivery of CPEs directly into the stratum corneum, these molecules are no longer limited by passive diffusion, thereby allowing them to induce increased chemical perturbation to the skin, in addition to the physical perturbation induced by the LFS treatment.

In spite of establishing that increased penetration and dispersion of CPEs in the skin induced by LFS is the origin of their synergism, to date, no direct mechanism has been proposed to explain *how* LFS increases the penetration of CPEs into the skin. Other studies have investigated the synergism between LFS and specific CPEs, such as SLS, more closely, and found that their simultaneous use induces subtle changes in the skin, such as altered pH profiles.[7] However, to our knowledge, no previous investigations have proposed a mechanism that explains why there is a general increase in the penetration of CPEs into the skin when treated simultaneously with LFS, which would explain this commonly observed synergism.

With the above in mind, in this study, we propose a plausible physical mechanism that explains why *all* CPEs are expected to exhibit synergism with LFS, as well as why surfactants, specifically, exhibit *greater* synergism with LFS than non-amphiphilic CPEs. In addition to proposing a physical mechanism, a kinetic-transport model is presented to explain the synergism quantitatively, by solving explicitly for the expected CPE flux into skin during LFS treatment, with supporting data from experiments conducted with both amphiphilic and non-amphiphilic CPEs.

2. EXPERIMENTAL SECTION

2.1 Materials

Sodium lauryl sulfate (SLS), octyl glucoside (OG), and propylene glycol (PG), were obtained from Sigma-Aldrich Company (St. Louis, MO). C_{14}-labeled SLS, OG, and PG were obtained from American Radiolabeled Chemicals (St. Louis, MO). Hionic-Fluor, a scintillation cocktail, and Soluene, a tissue solubilizer, were obtained from Perkin-Elmer (Waltham, MA). Allura red (red food coloring) was obtained from TCI America (Portland, OR). All chemicals were used as received. Milli-Q water (Millipore Corporation, Billerica, MA) was used for the preparation of all aqueous solutions.

2.2 Surface Tension Measurements

The surface tensions of aqueous solutions of the two amphiphiles, SLS and OG, were measured as a function of concentration using a Krüss K11 tensiometer (Hamburg,

Germany). The Wilhelmy-plate method was utilized with a titanium plate (Krüss, wetting length of 42 mm). For each measurement, twenty surface tension readings were obtained, three seconds apart, and the final ten readings were averaged to yield the surface tension for that measurement (with the first ten measurements serving as an equilibration period). Surface tension measurements of each solution considered were repeated until consistent values were obtained for three consecutive measurements (<0.1 mN/m variation). These three measurements were then averaged to yield the surface tension of the solution. The surface tension measurements were utilized to deduce the critical micelle concentration (CMC) of the surfactants, SLS and OG. This was accomplished by determining the intersection of the linear region below and above the CMC in a plot of surface tension vs. log surfactant concentration. [8]

2.3 Preparation and Treatment of Skin Samples by LFS and CPEs

Previously published protocols were utilized for the storage and preparation of skin samples. [9–16] These protocols have been approved by the MIT Committee on Animal Care. Briefly, skin was harvested from the back and flank of Female Yorkshire pigs, sectioned into 25-mm strips, and stored at −85 °C for up to 6 months. Before use in experiments, the skin was thawed for 1 hour in PBS and all excess hair and subcutaneous fat were removed. Full-thickness skin samples were utilized without further preparation. The skin was then cut into 25 mm by 25 mm samples, for use in the 15-mm inner diameter diffusion cells (PermeGear, Hellertown, PA).

Treatment of skin samples was carried out according to previously published methods. [10–16] Skin treatment was carried out with a 20 kHz ultrasound horn (VCX 500, Sonics and Materials, Inc., Newtown, CT), under the following experimental conditions: intensity − 7.5 W/cm^2, duty cycle – 100%, and tip displacement − 3 mm. The coupling solution between the skin and the ultrasound horn contained aqueous solutions of SLS (1– 100 mM), OG (4 – 100 mM), and PG (100– 700 mM) with 0.5 mM allura red (used for visualization of LTRs only, see Figure 1). The concentration of CPEs was selected so that they produced consistently large enough LTRs to allow sampling utilizing the techniques discussed in Section 2.4. Note that dilute allura red solutions have previously been shown not to interact strongly with other surfactants, or affect bulk or interfacial properties of aqueous surfactant solutions.[15] The concentration of radio-labeled permeant in the solutions was chosen to be between 0.–30.5 μCi/mL, in order to ensure that the fluxes of the radio-labeled materials into the skin were at a level which is significantly higher than the background values. After every 40 s of LFS treatment, the coupling medium (volume = 1.5 mL) was changed in order to minimize thermal effects (i.e., to maintain the temperature within 10 °C of room temperature), and samples were treated for a total of 10 minutes. Untreated skin samples were prepared in the same manner as other samples, but were contacted with the coupling solutions for 10 minutes without ultrasound treatment. Following treatment, samples were rinsed thoroughly in order to remove all excess material from the skin surface prior to sampling of the tissue.

2.4 Quantifying the Flux of CPEs into LTRs, non-LTRs, and Untreated Skin Samples

In order to quantify the amount of radio-labeled SLS, OG, and PG penetrating into the localized transport regions (LTRs, see Figure 1), the non-LTRs, and the untreated skin samples, samples were first blotted dry with lab tissue to remove all excess fluid on the surface of the skin. In samples treated with LFS, LTRs were identified visually because they were stained a deep red by the allura red dye, while non-LTRs were not stained to a noticeable extent (see Figure 1). In the timeframe of the experiments (10 minutes), permeants were not found to pass through the skin samples into the receiver compartment of the Franz diffusion cell. Therefore, the flux of permeant in each of the LTR and non-LTR

regions was sampled by simply removing that portion of the skin using a spherical cutting tool (similar to a hole-puncher).[17] Two diameters were utilized, 1 mm and 2.5 mm, depending on the area of the LTR being sampled. Non-LTRs were only sampled utilizing the 2.5 mm – diameter cutting tool, because these regions comprised larger areas of the skin surface. Note that this sampling method has been successfully utilized in previous studies for the quantification of radio-labeled permeants within LTRs and non-LTRs.[17] On each skin sample, it was typically possible to sample 2–5 LTR samples and 5–8 non-LTR samples (since the non-LTRs occupy larger areas on the skin), with a total of 8–10 samples typically taken from each piece of treated skin. The skin samples were then solubilized using Soluene-350 (1.5 mL), and the amount of radio-labeled permeant was quantified using a Tri-Carb Liquid Scintillation Counter (Perkin-Elmer), utilizing the scintillation cocktail Hionic-Fluor (5 mL). This process was repeated for 4–5 skin samples for each chemical penetration enhancer at each concentration tested. Untreated skin samples were contacted for 10 minutes with a coupling solution which was identical to that used in the previous treatments, but in the absence of LFS. For untreated samples, the entire skin sample that contacted the solution (with area of 1.77 cm^2) was used to quantify the amount of radio-labeled permeant in the skin. For the larger samples, 5 mL of Soluene-350 and 15 mL of Hionic-Fluor were utilized in the analysis of each sample. This process was repeated for 4–5 skin samples for each CPE considered at each concentration tested. For all samples, the concentration of the CPE was normalized by the surface area of that sample and by the application time (10 minutes = 600 s) in order to calculate the average flux into the skin in that area for the duration of the experiment. Note that in all the plots shown here, error bars correspond to 95% confidence intervals.

3. Theory

3.1 The Physical Picture

The underlying physical picture describing what occurs to the skin, and in the coupling medium above the skin, during LFS treatment has been the source of some debate in the literature. Specifically, although it is well established that transient cavitation plays a predominant role, [2] the location and type of transient cavitation responsible for skin perturbation are not agreed upon by all researchers in the field. For example, the ability of cavitation microjets to penetrate into the skin, as is observed when a physical dosimeter, such as aluminum foil, is utilized with low-frequency ultrasound, is not agreed upon universally. Because microscopy does not always provide direct evidence of microjet collapse into the skin, some researchers maintain that microjets do not penetrate into the skin, but rather perturb the skin in a less invasive manner. However, there is ample evidence to the contrary. First, although often overlooked, there *is* microscopy-based evidence of crater-like pores left in the skin following LFS treatment[18], thereby providing direct microscopy-based evidence of cavitation microjet penetration into the skin. Secondly, extensive recent work has shown that the effective aqueous pore radius of the skin increases when treated with LFS.[6, 11, 12, 16, 17] In particular, a recent study by our group closely evaluated the size of pores left in the LTRs and non-LTRs of LFS-treated skin.[17] In this study, we found that the effective aqueous pore radius scales directly with the trend that one would expect from direct microjet impingement into the skin *only* within LTRs. On the other hand, we found that aqueous pore radii were not dramatically affected within non-LTRs, suggesting that a less invasive mechanism, such as acoustic streaming, is responsible for increased permeant uptake in these skin regions (see Figure 2). Therefore, based on these findings, possible reasons why many microscopy-based studies have failed to observe pores left in the skin by LFS include: i) lower levels of LFS treatment (resulting in larger non-LTRs and smaller LTR areas on the skin surface), ii) imaging not being conducted within LTRs, and/or iii) the pores left in the skin not being large enough to be easily detected. More discussion on this topic can be found in [17].

The present study builds upon the findings of the research presented in [17] in order to better understand the mechanism by which CPEs and ultrasound interact to induce increased uptake of CPEs during LFS treatment, thereby shedding light on the synergism that these chemical and physical penetration enhancers share. As will be shown in Section 3.2, the presence of acoustic cavitation microjets has a pronounced impact on the flux of permeants into the skin within LTRs during LFS treatment.

3.2 Modeling the Flux of CPEs into the Skin

The synergism between LFS and CPEs, specifically surfactants, was previously shown to occur due to increased penetration and dispersion of these molecules in the skin.[3] However, no physical mechanism was proposed to explain *how* LFS induces greater penetration of surfactants and other CPEs into the skin. In this section, we will make use of the physical picture presented in Section 3.1 to model the fluxes of different types of CPEs into untreated skin samples and into the non-LTRs and LTRs of LFS-treated skin samples (see Figure 2). Through this analysis, the cause of increased CPE uptake into skin during LFS treatment will be clarified, thus shedding light on the origin of the synergism between LFS and CPEs, including why amphiphilic CPEs (such as SLS or OG) exhibit even greater synergism with LFS than non-amphiphilic CPEs (such as PG). Note that the flux equations that are derived in the following sections apply only to the delivery of CPEs into the skin during the initial, 10-minute LFS treatment. These equations should not be interpreted as being steady-state flux equations relevant to the delivery of drug compounds post-LFS treatment, or as being directly correlated to the overall steady-state skin permeability. Furthermore, note that this derivation is only valid for single CPEs in the LFS coupling medium, since the incorporation of multiple CPEs into the LFS coupling medium could lead to binary, or higher-order, interactions of these molecules in solution, a feature which is not considered in this study.

3.2.1 The Flux of Permeants into Untreated Skin—Modeling the flux of CPEs into untreated skin is straightforward. In this case, permeant flux into the skin, $J_{passive}$, is related directly to the bulk concentration of that species, C_b, by a diffusional mass-transfer coefficient, k_m. Note that we assume, throughout this paper, that the aqueous concentration just above the skin is much smaller than C_b, and therefore, we write the driving force for diffusion as C_b rather than as a concentration difference. Specifically,

$$J_{passive}=k_m C_b \tag{1}$$

If the permeant is amphiphilic (e.g., SLS or OG), and able to self-assemble into micelles, Eq. (1) needs to be modified to account for both monomeric and micellar species present in the coupling medium solution, because monomers and micelles have different mass-transfer coefficients relating their fluxes into the skin to the corresponding bulk concentrations. It is important to recognize that it is possible for micelles to penetrate into the skin as intact entities, as shown in prior research by our group.[19–21] Taking both monomers (*mon*) and micelles (*mic*) into account results in the following expression for $J_{passive}$, for the case of amphiphilic permeants above their CMC (the surfactant concentration beyond which micelles form):

$$J_{passive}=k_{m,mon}C_{CMC}+k_{m,mic}n_{agg}C_{b,mic} \tag{2}$$

where $k_{m,mon}$ is the mass-transfer coefficient of the amphiphilic monomers, C_{CMC} is the critical micelle concentration (CMC) of the surfactant, $k_{m,mic}$ is the mass-transfer coefficient of a monomer incorporated into a micelle, n_{agg} is the aggregation number of the micelles, and $C_{b,mic}$ is the bulk concentration of micelles in solution.

We can then relate $C_{b,mic}$ to the experimentally controllable variable C_b through the following relation:

$$C_{b,mic}=\left(\frac{C_b - C_{CMC}}{n_{agg}}\right) \tag{3}$$

Substituting Eq. (3) into Eq. (2) yields the following relation for the simultaneous flux of monomeric and micellar species into the skin:

$$J_{passive}=k_{m,mic}C_b+(k_{m,mon} - k_{m,mic})\,C_{CMC} \tag{4}$$

3.2.2 The Flux of Permeants into the Non-LTRs of Skin during LFS Treatment—As stated in Section 3.1, the flux of permeants into non-LTRs during LFS treatment is enhanced solely by a decrease in the bulk solution resistance due to an increase in stirring induced by acoustic streaming. Therefore, the expressions for the fluxes of monomers and micelles into non-LTRs of LFS-treated skin are similar to those in the untreated case, albeit with enhanced mass-transfer coefficients. In particular, for both non-amphiphilic and amphiphilic permeants below their CMC (where only monomers are present), the flux into the skin can be modeled as follows:

$$J_{non-LTR}=k_m^{'}C_b \tag{5}$$

where the prime indicates an enhanced mass-transfer coefficient.

Similar to the untreated case, above the CMC, when both monomers and micelles are present in solution, the resulting equation relating the overall non-LTR flux to the bulk concentration is given by:

$$J_{non-LTR}=k_{m,mic}^{'}C_b+\left(k_{m,mon}^{'} - k_{m,mic}^{'}\right)C_{CMC} \tag{6}$$

where the primes indicate enhanced mass-transfer coefficients.

3.2.3 The Flux of Permeants into the LTRs of Skin during LFS Treatment— Modeling the flux of permeants into the LTRs of skin during LFS treatment is not as straightforward as in the untreated or non-LTR cases, because the impingement of acoustic cavitation microjets within these regions must be accounted for, in addition to the convection-enhanced diffusional contribution to the flux. First, let us consider the case of a non-amphiphilic (NA) permeant, where adsorption of molecules onto the cavitation bubbles is not possible since they are not surface active. In this case, the flux of permeant into the skin depends on two contributions: (i) a convection-enhanced diffusional contribution, similar to that in the non-LTR case, and (ii) a contribution related to the amount of bulk fluid—injected into the skin as a result of each acoustic cavitation microjet collapse at the skin surface. Specifically, the amount of permeant delivered per microjet collapse is equivalent to the volume of bulk fluid transported into the skin per cavitation microjet collapse on the skin surface (v_{cav}) multiplied by cav the bulk concentration of that species (C_b). Including this contribution results in the following expression:

$$J_{LTR,NA}=\underbrace{k_m^{''}C_b}_{Diffusive\ Flux}+\underbrace{\dot{n}_{\mathrm{cav}}v_{\mathrm{cav}}C_b}_{Convective\ Flux} \tag{7}$$

where the double-prime indicates that the diffusive mass-transfer coefficient (k_m'') may be different from the diffusive mass-transfer coefficient (k_m' in the non-LTR case (see Eq. (5)) and $\dot{n}_{\text{cav}}$ is the number of acoustic cavitation microjet collapses per LTR area per unit time.

Collecting terms, Eq. (7) can be simplified as follows:

$$J_{LTR,NA} = \left(k_m'' + \dot{n}_{\text{cav}} v_{\text{cav}}\right) C_b \tag{8}$$

Equation (8) shows that the flux of non-amphiphilic species into the skin should be directly proportional to the bulk concentration, C_b, but to a much greater extent than in the untreated or non-LTR cases (see Eqs. (1) and (5)).

3.2.4 The Flux of Amphiphilic Permeants into the LTRs of Skin during LFS Treatment below their CMC—In the case of the surface-active amphiphilic permeants, an additional contribution to the flux must be accounted for—the amount of permeant that is adsorbed at the gas/water interface of the cavitation bubbles (see Figure 3). Note that previous sonochemical studies have established that there is an accumulation of surfactants at the gas/water interface of acoustic cavitation bubbles.[22]

For the case of amphiphilic (A) permeants below their CMC, we model their flux within LTRs by modifying Eq. (8) as follows:

$$J_{LTR,A} = \underbrace{k_m'' C_b}_{\text{Diffusive Flux}} + \underbrace{\dot{n}_{\text{cav}} v_{\text{cav}} C_b}_{\text{Convective Flux}} + \underbrace{\dot{n}_{\text{cav}} A_{cav} \Gamma}_{\text{Adsorptive Flux}} \tag{9}$$

where A_{cav} is the average surface area of an acoustic cavitation bubble, and Γ is the equilibrium concentration of surfactant species adsorbed at the cavitation bubble interface. The justification for the assumption that Γ is reaching equilibrium will be discussed in Section 4.3.1.

To find an expression for Γ, we will assume that only monomers can adsorb to, and desorb from, the gas/water interface (see Figure 4). In addition, because the quantity of permeant transported onto the cavitation bubbles and into the skin is small relative to the total permeant concentration in solution, the concentration of monomers and micelles in solution may be assumed to be constant. As a result, the equilibrium between monomers and micelles will be assumed to remain unperturbed at concentrations above the CMC (see Section 4.3.1). For simplicity, we will model the dependence of Γ on C_b utilizing Henry's adsorption isotherm, which is valid for dilute surface concentrations and has been previously used to model SLS adsorption at an air/water interface.[23, 24] This results in the following expression:

$$\Gamma = K_H C_b \tag{10}$$

where K_H is the Henry equilibrium adsorption constant for a given amphiphilic permeant, and is defined as $K_H = K_L \Gamma_\infty$, where K_L is the equilibrium adsorption coefficient of the amphiphile (defined as the ratio of the rate of amphiphile adsorption to the rate of amphiphile desorption, k_a/k_d, see Figure 4), and Γ_∞ is the maximum surface concentration of the amphiphile. The specific values of K_L and Γ_∞ are not important for our discussion and, therefore, the lumped K_H parameter will be utilized throughout the paper.

Substituting Eq. (10) into Eq. (9), the flux of the amphiphilic permeant into LTRs, below the CMC, is modeled as follows:

$$J_{LTR,A} = \underbrace{k_m'' C_b}_{Diffusive\ Flux} + \underbrace{\dot{n}_{cav} v_{cav} C_b}_{Convective\ Flux} + \underbrace{\dot{n}_{cav} A_{cav} K_H C_b}_{Adsorptive\ Flux} \quad (11)$$

Collecting terms, Eq. (11)) can be simplified as follows:

$$J_{LTR,A} = \left[k_m'' + \dot{n}_{cav} (v_{cav} + A_{cav} K_H) \right] C_b \quad (12)$$

Equation (12) indicates that the flux of amphiphilic permeants into LTRs during LFS treatment, below their CMC, should be even greater than that of non-amphiphilic permeants (see Eq. (8)).

3.2.5 The Flux of Amphiphilic Permeants into the LTRs of Skin during LFS Treatment Above their CMC—Because micelles cannot directly adsorb at the gas/water interface of cavitation bubbles, the model must be modified above the CMC to account for the presence of both monomers and micelles. Using Eq. (6) to model the diffusive flux above the CMC and now holding the concentration of monomers constant at the CMC, one obtains:

$$J_{LTR,A} = \underbrace{k_{m,mic}'' C_b + \left(k_{m,mon}'' - k_{m,mic}'' \right) C_{CMC}}_{Diffusive\ Flux} + \underbrace{\dot{n}_{cav} v_{cav} C_b}_{Convective\ Flux} + \underbrace{\dot{n}_{cav} A_{cav} K_H C_{CMC}}_{Adsorptive\ Flux} \quad (13)$$

where the double-prime indicates that $k_{m,mic}''$ and $k_{m,mon}''$ may be different from $k_{m,mic}'$ and $k_{m,mon}'$.

Collecting terms, Eq. (13) can be simplified as follows:

$$J_{LTR,A} = \left[\left(k_{m,mon}'' - k_{m,mic}'' \right) + \dot{n}_{cav} A_{cav} K_H \right] C_{CMC} + \left(k_{m,mic}'' + \dot{n}_{cav} v_{cav} \right) C_b \quad (14)$$

Note that the slope of the $J_{LTR,A}$ vs. C_b curve is equal to that corresponding to a non-amphiphilic species in Eq. (8). This result will be analyzed further in Section 4.3.2.

3.2.6 Summary of Expected Trends in the Flux Data—As shown in Sections 3.2.1–3.2.2, the flux of both amphiphilic and non-amphiphilic species into untreated skin and the non-LTRs of skin during LFS treatment should follow similar trends (see Section 4.1). However, due to the enhanced stirring induced by acoustic streaming, the flux into the non-LTRs should be enhanced relative to that into untreated skin (compare Eqs. (1) and (4) to Eqs. (5) and (6)). This suggests that the slope observed for the flux vs. bulk concentration curve should be greater in the non-LTR case than in the case of untreated skin. Within LTRs during LFS treatment, the expected flux of non-amphipihlic permeants should be dominated by a convective term associated with the collapse of acoustic cavitation microjets (see Section 4.2). Furthermore, for amphiphilic permeants below their CMC (amphiphilic monomers), the flux into the LTRs during LFS treatment is expected to be further enhanced due to the adsorption of the amphiphiles onto the surface of cavitation bubbles (see Section 4.3). However, above the CMC of amphiphilic permeants, the slope of the flux vs. bulk concentration curve should revert to a value which is similar to that of a non-amphiphilic molecule because micelles are not able to adsorb at the surface of cavitation bubbles (see Eqs. (8) and (14)).

It is now apparent that the origin of the increase in the penetration of CPEs into the skin induced by LFS, and consequently their synergism, results from the cavitation-related convective and adsorptive contributions to the flux. Specifically, the flux into the LTRs of any permeant that acts as a CPE will be enhanced by the convective flux contribution. In addition, the flux of amphiphilic permeants (e.g., surfactants) will be enhanced even further due to their ability to adsorb at the surface of acoustic cavitation bubbles, thereby generating an even greater flux into the skin. The concepts of convective and adsorptive fluxes will be tested in the Results and Discussion section by utilizing a non-amphiphilic CPE, propylene glycol (PG), and two amphiphilic CPEs, sodium lauryl sulfate (SLS, an anionic surfactant) and octyl glucoside (OG, a nonionic surfactant). The simplifications and assumptions made in the derivation of the flux model presented in Section 3 will be analyzed and justified in Section 4.3.1.

4. RESULTS AND DISCUSSION

To test the flux model presented in Section 3, the fluxes of three CPEs into the skin were tested, in both untreated skin and during LFS treatment of skin. LFS-treated skin samples consisted of both LTRs and non-LTRs (see Figure 1), and each of the regions were sampled as discussed in Section 2.4. The first CPE tested was PG, a non-amphiphilic, low-molecular weight (MW = 76 Da) molecule that is completely miscible in water. The other two CPEs, SLS and OG, are both amphiphilic molecules. Specifically, SLS is an anionic surfactant (MW = 288 Da), whose micelles have an aggregation number of ~60, [25] indicating that SLS micelles have a molecular weight of about 17 kDa. OG is a nonionic surfactant (MW = 292 Da), whose micelles have an aggregation number of ~90, [26] indicating that OG micelles have a molecular weight of about 26 kDa.

4.1 Flux of Permeants into Untreated Skin and the Non-LTRs of Skin During LFS Treatment

As discussed in Section 3.2.1, the flux of any given monomeric permeant into untreated skin is expected to be directly proportional to the bulk permeant concentration in solution, as related by a mass-transfer coefficient, k_m, which is specific to that permeant (see Eq. (1)). If micelles are present in solution, both amphiphiles in monomeric and micellar states are expected to have different mass-transfer coefficients ($k_{m,mon}$ and $k_{m,mic}$, respectively), with the amphiphilic molecules present within micelles expected to have decreased mobility relative to the monomers (that is, $k_{m,mon} > k_{m,mic}$). The fluxes of monomeric and micellar permeants into the non-LTRs of skin samples during LFS treatment are expected to follow the same trend as in untreated skin, but with enhanced mass-transfer coefficients ($k'_{m,mon}$ and $k'_{m,mic}$, respectively), as a result of the decreased bulk resistance due to enhanced stirring caused by acoustic streaming (see Section 3.1). The flux of PG, OG, and SLS into untreated skin and the non-LTRs of skin during LFS treatment are shown in Figures 5, 6, and 7, with the corresponding mass-transfer coefficients calculated from these plots summarized in Table 1. Recall that for the amphiphilic permeants (OG and SLS), the slope below the CMC is equivalent to $k_{m,mon}$ for the untreated skin samples and to $k'_{m,mon}$ for the non-LTR samples. Similarly, the slope above the CMC is equivalent to $k_{m,mic}$ for the untreated skin samples and to $k'_{m,mic}$ for the non-LTR samples. In the analysis of the data, the y-intercept of the linear regressions for the non-amphiphilic permeant (PG), as well as for the amphiphilic permeants (OG and SLS) below their CMC, were forced to zero, because a non-zero y-intercept has no physical meaning in the context of the flux model. The CMC's of OG and SLS were found experimentally to be 18 mM and 7.7 mM, respectively, utilizing surface tension measurements (see Section 2.2). Note that there is good agreement between the break in the flux curves shown in Figures 6 and 7 and the experimentally deduced CMC values, as is expected within the formulated flux model.

Figures 5–7, as well as Table 1, show that the untreated skin and non-LTR data follow the trends predicted in Sections 3.2.1 and 3.2.2, respectively. In other words, for each permeant considered, the flux vs. bulk concentration curves follow similar trends in both the untreated and non-LTR skin samples, with an enhancement observed in the non-LTR samples relative to the untreated samples. In the case of the nonionic permeants, the mass transfer coefficients increase by approximately one order-of-magnitude for both PG and OG monomers, as well as for the OG micelles, in the non-LTR samples relative to the untreated skin samples (see Table 1). For SLS monomers and micelles, the increase in the mass-transfer coefficients between the non-LTR samples and the untreated skin samples is about 4-fold in each case (see Table 1). The increase in the flux of SLS in the non-LTRs relative to the untreated skin samples is less than in the case of the nonionic species because: (i) both the skin and SLS are negatively charged, and therefore, partitioning of the ionic molecules into the skin may be a limiting factor, and (ii) $k_{m,mon}$ and $k_{m,mic}$ are larger for SLS than for PG and OG (see Table 1), and, as a result, there may be less inherent bulk resistance to SLS flux into the skin, which would result in acoustic streaming having a less significant role in increasing the mass-transfer coefficients of SLS into the non-LTRs of LFS-treated skin.

4.2 Flux of Non-Amphiphilic Permeants into the LTRs of Skin during LFS Treatment

As shown in Section 3.2.3, the flux into the LTRs of skin during LFS treatment depends on the amount of material delivered into the skin due to the impingement of microjets in these regions (as reflected in $\dot{n}_{cav} \cdot v_{cav}$), in addition to a less significant diffusive flux term (k_m''). This cavitation-related contribution is effectively a convective flux, and therefore may be expressed as follows:

$$J_V = V \cdot C_b \tag{15}$$

where V is an effective convective velocity associated with the impingement of microjets and is equivalent to $\dot{n}_{cav} \cdot v_{cav}$, in terms of the variables defined previously. Therefore, regardless of the size of the permeant being delivered, this convective flux contribution should be constant as long as the cavitation field remains constant (i.e., $\dot{n}_{cav}$ and v_{cav} do not change) and there is no additional flux associated with the adsorption of molecules to the cavitation bubbles (as is the case for amphiphilic permeants).

The flux of PG into the LTRs of LFS-treated skin as a function of PG bulk concentration is presented in Figure 8. Figure 8 shows that as predicted by the flux model for this non-amphiphilic molecule, the data is linear (see Eq. (12)), but with a much larger flux than in the case of the non-LTRs (see Eq. (5)). Because the LTRs and the non-LTRs were sampled from the same pieces of skin (both LTRs and non-LTRs are present on LFS-treated skin samples, see Figure 1), we can gauge the importance of the convective contribution relative to that of the diffusive contribution by assuming $k'_{m,PG} \sim k''_{m,PG}$. Making this assumption, it follows that the slope in Figure 8, $5.1 \cdot 10^{-7}$ *m*/*s* (see Table 2), is over an order-of-magnitude greater than $k'_{m,PG}$ ($4.6 \cdot 10^{-8}$ *m*/*s*, see Table 1). Accordingly, to leading order, the flux of PG into the LTRs of LFS-treated skin is proportional to the convective contribution. Therefore, to a good approximation, we can assume that the diffusive contribution to the flux is negligible in the LTRs (see Eq. (7)), and that the flux of non-amphiphilic permeants into the LTRs is given by:

$$J_{LTR,NA} = \dot{n}_{cav} v_{cav} \cdot C_b = V \cdot C_b \tag{16}$$

Furthermore, in the context of our flux model, it is important to recognize that the flux of amphiphilic permeants into the LTRs of skin during LFS treatment, above their CMC,

exhibits the same dependence on the permeant bulk concentration as do non-amphiphilic permeants Accordingly, Eq. (16) will become useful in analyzing the OG and SLS data at concentrations above the CMC for each permeant, and in supporting our flux model (see Section 4.3.2).

4.3 Flux of Amphiphilic Permeants into the LTRs of Skin during LFS Treatment

As discussed in Section 3, in addition to the convective contribution to the flux, which is significant within the LTRs, an adsorptive contribution to the flux must also be included to model the flux of amphiphilic species within LTRs during LFS treatment. This is due to the fact that amphiphiles can adsorb to the surface of cavitation bubbles and be transported into the skin, in addition to being delivered into the skin due to convection induced by the impingement of acoustic cavitation microjets.

4.3.1 Assumptions of the Model—In order to estimate the concentration of adsorbed amphiphiles in the context of our flux model, we implemented the following simplifying assumptions.

1. The concentrations of bulk monomers, $C_{b,mon}$, and bulk micelles, $C_{b,mic}$, are constant in the LFS coupling solution, and therefore, equilibrium between these two species is maintained throughout the LFS treatment.

   - In order to test this assumption, the amount of permeant that is transported into the skin was compared to the total amount of permeant in the LFS coupling solution. Typically, the total surface coverage of LTRs is 5–20% and that of non-LTRs is 80–95%. Because more permeant enters LTRs than non-LTRs, assuming that 20% of the skin samples contain LTRs should provide an upper threshold estimate. Multiplying the LTR fluxes found in Figures 8–10 and the non-LTR fluxes found in Figures 5–7 by the treatment time (600 s) and the skin surface area of each region (having a total area of 177 mm^2), we find that for both OG and SLS, the upper threshold for the amount of permeant transported into the skin is less than 1% of that in the bulk solution, thereby validating assumption 1.

2. The cavitation bubbles are at adsorption equilibrium when collapsing at the skin surface.

   - In order to test this assumption, one must compare the lifetime of an average cavitation bubble with the time scale associated with monomer adsorption onto a cavitation bubble. The average velocity of cavitation bubbles at 20 kHz, generated using equipment which is similar to the one utilized in the present study, was reported to be 1.007 m/s.[27] In our experiments, the ultrasound horn is positioned 3 mm from the skin surface. Therefore, taking the characteristic length scale to be of order 1 mm, we find that the average bubble lifetime is on the order of 1 ms. In the context of Henry's adsorption isotherm used in our analysis, the relevant adsorption parameters could only be found for SLS. Specifically, taking into account the characteristic length scale of SLS adsorption (the distance an SLS molecule must travel in the bulk solution to adsorb to the gas/water interface), which is reported to be of the order $1{\cdot}10^{-7}$ *m*, [23] and the rate of SLS adsorption (k_a), which was reported to range between $5.5{\cdot}10^{-4}$–3 *m/s* below the CMC, [24] we estimated that the timescale for adsorption of SLS onto the cavitation bubbles is ~0.03–180 μs, which is significantly faster than 1 ms. It then follows that our equilibrium assumption (assumption 2) is valid, since the timescale for adsorption is much faster than the average lifetime of a bubble.

3. As stated in Section 3, the derivation of the flux model assumes that the cavitation field parameters, $\dot{n}_{cav}$, v_{cav}, and A_{cav}, do not vary significantly during our

experiments. In this respect, sonochemical research has shown that there is not much dependence of sonoluminescense and other indicators of the cavitation field at low frequencies (e.g., 20 kHz).[28] For example, the presence of methacrylic acid (a small organic compound that is soluble in both water and organic solvents), at concentrations up to 65 mM, was shown to only decrease sonoluminescense on the order of 10% at 20 kHz. Moreover, surface tension effects have also been shown to not greatly affect indicators of the cavitation field, such as sonoluminescence.[29] Therefore, at the operating frequency used in the present study (20 kHz), assumption 3 is reasonable.

4.3.2 Fluxes of OG and SLS into the LTRs of Skin during LFS Treatment—As discussed in Section 3.2.3, the flux of amphiphilic permeants into LTRs, below their CMC, should be larger than that of non-amphiphilic permeants, because of the additional contribution of the surface adsorptive flux (see Eq. (11)). As the amphiphilic permeant concentration increases beyond its CMC, the slope of the flux vs. bulk concentration curve should revert to that expected for a non-amphiphilic permeant, as shown in Eq. (16), because micelles cannot adsorb onto the surface of cavitation bubbles.

Figures 9 and 10 show that the fluxes of both OG and SLS, below their CMC's, are greater than the flux of PG (compare the data points to the dashed lines in Figures 9 and 10). This follows from our flux model (compare Eqs. (9) and (7)) because the flux of amphiphilic permeants into the skin over this concentration range depends on both the adsorptive flux and the convective flux. By comparing the slopes of the OG and SLS data to the slope of the PG data (see Table 2), it follows that the adsorptive flux accounts for 30% of the OG flux into the skin and 73% of the SLS flux into the skin below the CMC for each amphiphile. In the context of our flux model, the difference in the slopes of the OG and SLS data below the CMC of each amphiphile reflects the different K_H values associated with each amphiphile (see Eq. (12)). Further discussion about the kinetic adsorption parameters of OG and SLS is presented in Section 4.3.3.

However, as predicted by our flux model (see Eq. (16)), the slopes above the CMC's of both OG and SLS are nearly identical to that of the PG data (within 10% error, see Table 2). This indicates that both small molecules, such as OG (MW = 76 Da), and large micellar aggregates (MW = 17–26 kDa) are transported into the skin at nearly the same rate! This result is indicative of convective transport (see Eq. (15)), which in this case results from the collapse of acoustic cavitation microjets, and fits the expected trends of our flux model. It is important to stress that, for the SLS data presented in Figure 10, our flux model no longer fits the data at and above a threshold SLS concentration of 65 mM, since the data falls below the predicted trend line. Because the flux model still holds at similar concentrations of the nonionic amphiphile OG (see Figure 9), it is likely that electrostatic effects may be the cause of the observed deviation from the flux model above a threshold concentration for the charged, anionic SLS amphiphile. Further analysis and discussion of this deviation is presented in Section 4.3.4.

4.3.3 Analysis of Kinetic and Cavitation-Related Variables Deduced from the Flux Model—Equation (13) derived in Section 3.2.3 to model the flux of permeants into the LTRs of skin during LFS treatment contains four variables, n_{cav}, v_{cav}, A_{cav}, and K_H, of which the species-specific K_H variable is only relevant for amphiphilic permeants. Therefore, given that there are a total of *five* unknown variables (including K_H for OG and SLS) and we have a total of three equations relating them (those corresponding to PG, OG, and SLS), we need to accurately estimate two variables in order to be able to fully define the system. This analysis is critical in determining whether the quantitative values derived from the flux model are realistic, and therefore in further substantiating our flux model.

A logical starting point in our analysis involves estimating the two variables that depend on the size of the cavitation bubbles, v_{cav} and A_{cav}. Specifically, v_{cav} is the volume of bulk fluid delivered into the skin by each collapsing cavitation bubble, and A_{cav} is the average surface area of a cavitation bubble. Therefore, we will first relate v_{cav} and A_{cav} to the average cavitation bubble radius to eliminate one unknown. We begin by analyzing the dependence of v_{cav} on the average size of a cavitation bubble before it collapses onto the skin. To leading order, the simplest scenario assumes that the amount of volume that a cavitation bubble delivers into the skin is directly proportional to the volume of fluid that it displaces in solution. In other words, for a spherical cavitation bubble v_{cav} and R_{cav} are simply related as follows:

$$v_{cav}=\frac{4}{3}\pi R_{cav}^3 \tag{17}$$

where R_{cav} is the average radius of a cavitation bubble prior to its collapse on the skin surface.

Similarly, the average surface area of a cavitation bubble is related to R_{cav} as follows:

$$A_{cav}=4\pi R_{cav}^3 \tag{18}$$

Equations (17) and (18) allow us to express v_{cav} and A_{cav} in terms of the single variable, R_{cav}. Therefore, if we can estimate R_{cav}, we can solve explicitly for the three equations corresponding to the fluxes of PG, OG, and SLS into LTRs. Interestingly, a previous study conducted using similar equipment to the one used here, at 20 kHz, found that the number average diameter of cavitation bubbles is 6.3 μm, corresponding to a number average radius of 3.15 μm.[27] Using this R_{cav} value in Eq. (17), we find that:

$$v_{cav}=\frac{4}{3}\pi R_{cav}^3=\frac{4}{3}\pi\left(3.15\cdot 10^{-6}m\right)^3=1.31\cdot 10^{-16}m^3 \tag{19}$$

Utilizing the PG data, we can next substitute v_{cav} from Eq. (19) in Eq. (16), utilizing the slope of the PG curve reported in Table 2, to solve for $\dot{n}_{cav}$ as follows:

$$\dot{n}_{cav}=\frac{\frac{J_{LTR,NA}}{C_b}}{v_{cav}}=\frac{PG\ slope}{v_{cav}}=\frac{\dot{n}_{cav}\cdot v_{cav}}{v_{cav}}=\frac{5.1\cdot 10^{-7}m/s}{1.31\cdot 10^{-16}m^3}microjets=3.9\cdot 10^9\frac{microjets}{m^2\cdot s} \tag{20}$$

Our group has previously reported that typical LTR areas formed at 20 kHz during a 10 minute treatment at an US intensity of 7.5 W/cm^2 are 10–40 mm^2 (for a sample having a total area of 177 mm^2, such as the one considered here).[10] Accordingly, our data suggests there are on the order of 10^7 cavitation bubble collapses into LTRs during a typical 10-minute ultrasound treatment at the conditions examined here.

Next, we consider the remaining two unknown variables, $K_{H,OG}$ and $K_{H,SLS}$, the equilibrium adsorption coefficients for OG and SLS, respectively. Substituting the slopes of the OG and SLS curves below their CMC (see Table 2), in addition to A_{cav} from Eq. (18) and the values of v_{cav} and $\dot{n}_{cav}$ calculated in Eqs. (19) and (20), respectively, in the expression for the expected slope for amphiphilic permeants below the CMC, $\dot{n}_{cav}$ (v_{cav} + $A_{cav}K_H$), yields:

$$\text{For OG:}\quad 7.3\cdot10^{-7}m/s=3.9\cdot10^{9}\frac{microjets}{m^2\cdot s}\left[1.3\cdot10^{-16}m^3+4\pi\left(3.15\cdot10^{-6}m\right)^2\cdot K_{H,OG}\right] \tag{21}$$

$$\text{For SLS:}\quad 1.9\cdot10^{-6}m/s=3.9\cdot10^{9}\frac{microjets}{m^2\cdot s}\left[1.3\cdot10^{-16}m^3+4\pi\left(3.15\cdot10^{-6}m\right)^2\cdot K_{H,OG}\right] \tag{22}$$

Solving Eqs. (21) and (22) results in values of $K_{H,OG} = 4.6\cdot10^{-7}$ *m* and $K_{H,SLS} = 2.9\cdot10^{-6}$ *m*. Because OG has not been studied as widely as SLS, typical $K_{H,OG}$ values for the adsorption of OG onto a static, planar air/water interface could not be found in the literature. Therefore, to verify that our data is reasonable, we will compare the $K_{H,SLS}$ values deduced from our experiments to reported literature values of the equilibrium SLS adsorption rate to a static, planar air/water interface, $K^{\exp}_{H,SLS}$. Typical values for $K^{\exp}_{H,SLS}$ are reported to be between 1.1–$1.5\cdot10^{-6}$ *m*.[23] We therefore find that the $K_{H,SLS}$ value deduced from our experimental data is slightly larger than the previously reported values corresponding to adsorption to a stagnant, planar interface. Recognizing that our calculation of $K_{H,SLS}$ made use of several assumptions, our estimated values of $K_{H,SLS} = 2.9\cdot10^{-6}$ *m*, is generally consistent with the reported literature values. For example, if the average cavitation bubble radius was one half of the values assumed here (3.15 μm), that is if R_{cav} =1.6 μm, then the estimated $K_{H,SLS}$ value would be $1.5\cdot10^{-6}$ *m* and fully consistent with the range of $K^{\exp}_{H,SLS}$ values reported in the literature. In fact, it is reasonable that the cavitation bubbles present in our system may be smaller than those previously reported in [27] because the distance from the ultrasound transducer at which the reported bubble diameters were measured was 30 mm. On the other hand, in our experiments, the distance between the ultrasound transducer and the skin surface is only 3 mm. Accordingly, cavitation bubbles in our system have less time to grow by rectified diffusion and should possess smaller radii. Moreover, the fact that the $K_{H,SLS}$ value found here is in general agreement with the $K^{\exp}_{H,SLS}$ literature values is also consistent with the reported observation that the kinetics of SLS adsorption onto an air/water interface is adsorption-rate limited and not diffusion-rate limited.[24] Therefore, the convective processes associated with the applied ultrasound field should not have a significant effect on the adsorption of SLS monomers onto the cavitation bubble surface.

4.3.4 Deviation of the Experimental Data from the Flux Model beyond a Threshold Concentration in the Case of Charged Amphiphiles (SLS)—As discussed in Section 4.3.2, for the charged, anionic amphiphile SLS, the expected LTR flux data deviates from that predicted by our flux model (at concentrations at and above 65 mM, see Figure 10). Because the observed deviation from the expected flux model prediction is only observed for the case of the ionic SLS, electrostatic effects are the probable cause for this deviation. In order to further rationalize the observed deviation, we first must identify what assumptions in our flux model may change if electrostatic effects are present. Examination of Eq. (14) reveals that n_{cav} and v_{cav} are the only variables related to the cavitation field that appears in the slope of the flux equation for amphiphilic permeants above their CMC. We would like to stress, before proceeding any further, that in nearly all ultrasound experimental treatment protocols, including clinical uses of this technology, [30] the concentration of SLS used is 1 wt% (35 mM) or lower. Therefore, operating in the SLS concentration region where deviation from the expected flux model prediction is observed (>65 mM) is not typical.

Previous sonochemical studies have investigated the effect of amphiphiles, including SLS, on the activity and properties of acoustic cavitation bubbles.[28, 29, 31, 32] Some of these

studies have even compared the effect of ionic and nonionic amphiphiles, revealing the importance of electrostatic effects.[31] Specifically, at low ionic concentrations (1–2 mM), without added salt, charging the surface of a cavitation bubble with ionic amphiphiles can produce stabilization and repulsive effects between bubbles. This phenomenon was likely not observed in our experiments because we only conducted measurements at one data point in this range (1 mM). However, the presence of an electrolyte (either in the form of an added ionic amphiphile or through the addition of other salts) can result in electrostatic screening which can have the inverse effect. This phenomenon has been studied with SLS at 1 mM. [29] Specifically, it was found that with 1 mM SLS in water (Debye screening length ~ 10 nm, see Figure 11), electrostatic repulsions between negatively-charged cavitation bubbles were able to inhibit bubble coalescence. However, when 100 mM sodium chloride was added to the SLS solution, decreasing the Debye screening length to ~ 1 nm, the secondary Bjerknes (attractive) force was found to dominate. Therefore, the authors concluded that at high ionic concentrations, Bjerknes (attractive) forces dominate, which may allow for bubble coalescence to take place.[29] In our system, no salt is added. Therefore, the only mechanism leading to a decrease in the Debye screening length, and an associated shift in bubble coalescence, is the addition of more negatively-charged SLS to the coupling solution. The Debye screening length, κ^{-1}, is defined as follows: [8]

$$\kappa^{-1}=\left[\left(\frac{e_0^2}{\varepsilon k_B T}\right)\sum_i z_i^2 n_{i\infty}\right]^{-\frac{1}{2}} \tag{23}$$

where e_0 is the electronic charge ($1.6\cdot10^{-19}$ *C*), $\varepsilon = \varepsilon_0\varepsilon_r$ is the dielectric permittivity of the medium ($\varepsilon_0=8.85\cdot10^{-12}\frac{C^2}{J\cdot m}$; for water, ε_r = 78.54), k_B is the Boltzmann constant ($1.38\cdot10^{-23}$ *J/K*), *T* is the absolute temperature, z_i is the valence of species *i*, $n_{i\infty}$ is the bulk concentration of species *i*, and *i* indicates that the summation is over all ionic species. Note that κ^{-1} is a property of the solution and is independent of the properties of the cavitation bubbles present in the solution.

Assuming complete dissociation of SLS, Figure 11 shows the dependence of κ^{-1} on bulk SLS concentration. Figure 11 shows that a value of κ^{-1} =1 nm is only approached at bulk SLS concentrations which are equal to or exceed 65 mM, corresponding to the threshold SLS concentration beyond which our flux model prediction begins to deviate from the experimental flux data (see Figure 10). Therefore, it is plausible that the cavitation-related parameters, $\dot{n}_{\mathrm{cav}}$ and v_{cav} , which were assumed to be constant in our flux model may begin to change at SLS concentrations above this threshold due to increased bubble coalescence. One possible explanation could be that increased coalescence of cavitation bubbles in the bulk solution may lead to instability and collapse of the cavitation bubbles prior to reaching the skin surface. In that case, the efficiency of bubble transfer to the skin surface may be decreased, thereby decreasing the number of cavitation bubbles collapsing at the skin surface. Such a process would result in a decrease in the flux of SLS into the skin (lower $\dot{n}_{\mathrm{cav}}$), as reflected in our flux data beyond concentrations of 65 mM (see Figure 10).

5. CONCLUSIONS

In this paper, we present a plausible physical mechanism The dashed, horizontal line corresponds to a value of 1 nm. that can explain how LFS increases the transdermal uptake of CPEs. Specifically, our findings suggest that the origin of the observed synergism between LFS and CPEs is the ability of LFS to increase the penetration and dispersion of CPEs by direct deposition of permeants into the LTRs of skin during LFS treatment through

the collapse of acoustic cavitation microjets. Moreover, amphiphilic permeants exhibit even greater synergism with LFS than non-amphiphilic permeants because their flux into the skin is further enhanced by the adsorption of amphiphilic monomers to the surface of the cavitation bubbles. Therefore, in addition to a convective flux induced by the collapse of acoustic cavitation microjets that drives all CPEs, amphiphilic CPEs adsorbed to cavitation bubbles are also *directly deposited* into the skin. More modest increases in the uptake of CPEs into the non-LTRs of LFS-treated skin, relative to untreated skin, were also observed (as predicted recently[17]) and are consistent with the prediction of our flux model.

The elucidation of the mechanism of deposition of amphiphilic CPEs into skin during LFS treatment may help to explain other interesting phenomena reported in the literature. For example, in some cases, extreme synergism or antagonism in skin permeability enhancement has been reported between LFS and binary mixtures of surfactants. [4] In the context of the findings here, synergism in these cases may be due to more efficient adsorption or packing of multiple surfactants on the surface of cavitation bubbles, while antagonism may be a result of decreased adsorption onto cavitation bubbles. Moreover, these trends may depend on the monomer concentration of each amphiphile in solution, since we have shown that only monomers can adsorb at the surface of cavitation bubbles. Therefore, a dramatic decrease in the CMC of binary surfactant mixtures may lead to antagonism between the surfactants comprising the mixtures, while an increase in the CMC may explain an even stronger synergism with LFS.

Accordingly, an exciting area of future research may involve testing the flux of binary surfactant mixtures into the LTRs of LFS-treated skin. Additional areas of experimentation that may also be of interest include further testing of charged surfactants, including cationic or zwitterionic surfactants, to further confirm the trends observed here with SLS (anionic) and OG (nonionic).

Acknowledgments

The authors thank Jaisree Iyer for insightful discussions on electrostatics of colloidal systems during the preparation of this manuscript. This work was funded by the National Institutes of Health (Grant# EB-00351) and the U.S. Army Research Office through the Institute for Solider Nanotechnologies at MIT (Grant# DAAD-19-02-D-002). The contents of this manuscript represent solely the views of the authors and do not necessarily reflect the position of the U.S. Government. No official endorsement should be inferred.

References

1. Polat BE, Blankschtein D, Langer R. Low-frequency sonophoresis: application to the transdermal delivery of macromolecules and hydrophilic drugs. Expert Opin Drug Del. 2010; 7(12):1415–1432.
2. Polat BE, Hart D, Langer R, Blankschtein D. Ultrasound-mediated transdermal drug delivery: Mechanisms, scope, and emerging trends. Journal of Controlled Release. 2011; 152(3):330–348. [PubMed: 21238514]
3. Mitragotri S, Ray D, Farrell J, Tang H, Yu B, Kost J, Blankschtein D, Langer R. Synergistic effect of low-frequency ultrasound and sodium lauryl sulfate on transdermal transport. J Pharm Sci. 2000; 89(7):892–900. [PubMed: 10861590]
4. Tezel A, Sens A, Tuchscherer J, Mitragotri S. Synergistic effect of low-frequency ultrasound and surfactants on skin permeability. J Pharm Sci. 2002; 91(1):91–100. [PubMed: 11782900]
5. Paliwal S, Menon G, Mitragotri S. Low-frequency sonophoresis: ultrastructural basis for stratum corneum permeability assessed using quantum dots. J Invest Dermatol. 2006; 126(5):1095–1101. [PubMed: 16528354]
6. Polat BE, Seto JE, Blankschtein D, Langer R. Application of the aqueous porous pathway model to quantify the effect of sodium lauryl sulfate on ultrasound-induced skin structural perturbation. Journal of pharmaceutical sciences. 2011; 100(4):1387–1397.

7. Lavon I, Grossman N, Kost J. The nature of ultrasound-SLS synergism during enhanced transdermal transport. J Control Release. 2005; 107(3):484–494. [PubMed: 16165244]
8. Hiemenz, P.; Rajagopalan, R. Principles of Colloid and Surface Chemistry. Marcel Dekker, Inc; New York: 1997.
9. Seto JE, Polat BE, VanVeller B, Lopez RFV, Langer R, Blankschtein D. Fluorescent penetration enhancers for transdermal applications. Journal of Controlled Release. 2011 in press. 10.1016/j.jconrel.2011.10.018
10. Kushner J, Blankschtein D, Langer R. Experimental demonstration of the existence of highly permeable localized transport regions in low-frequency sonophoresis. J Pharm Sci. 2004; 93(11): 2733–2745. [PubMed: 15389675]
11. Kushner J, Blankschtein D, Langer R. Evaluation of the porosity, the tortuosity, and the hindrance factor for the transdermal delivery of hydrophilic permeants in the context of the aqueous pore pathway hypothesis using dual-radiolabeled permeability experiments. J Pharm Sci. 2007; 96(12): 3263–3282. [PubMed: 17887176]
12. Kushner J, Blankschtein D, Langer R. Evaluation of hydrophilic permeant transport parameters in the localized and non-localized transport regions of skin treated simultaneously with low-frequency ultrasound and sodium lauryl sulfate. J Pharm Sci. 2008; 97(2):906–918. [PubMed: 17887123]
13. Kushner J, Kim D, So P, Blankschtein D, Langer R. Dual-channel two-photon microscopy study of transdermal transport in skin treated with low-frequency ultrasound and a chemical enhancer. J Invest Dermatol. 2007; 127(12):2832–2846. [PubMed: 17554365]
14. Lopez R, Seto J, Blankschtein D, Langer R. Enhancing the transdermal delivery of rigid nanoparticles using the simultaneous application of ultrasound and sodium lauryl sulfate. Biomaterials. 2011; 32(3):933–941. [PubMed: 20971504]
15. Polat BE, Lin S, Mendenhall JD, VanVeller B, Langer R, Blankschtein D. Experimental and Molecular Dynamics Investigation into the Amphiphilic Nature of Sulforhodamine B. The Journal of Physical Chemistry B. 2011; 115(6):1394–1402. [PubMed: 21222449]
16. Seto J, Polat B, Lopez R, Blankschtein D, Langer R. Effects of ultrasound and sodium lauryl sulfate on the transdermal delivery of hydrophilic permeants: Comparative in vitro studies with full-thickness and split-thickness pig and human skin. J Control Release. 2010; 145(1):26–32. [PubMed: 20346994]
17. Polat BE, Figueroa PL, Blankschtein D, Langer R. Transport pathways and enhancement mechanisms within localized and non-localized transport regions in skin treated with low-frequency sonophoresis and sodium lauryl sulfate. Journal of pharmaceutical sciences. 2011; 100(2):512–529. [PubMed: 20740667]
18. Yamashita N, Tachibana K, Ogawa K, Tsujita N, Tomita A. Scanning electron microscopic evaluation of the skin surface after ultrasound exposure. Anat Rec Part A. 1997; 247(4):455–461.
19. Ghosh S, Blankschtein D. Why is sodium cocoyl isethionate (SCI) mild to the skin barrier? An in vitro investigation based on the relative sizes of the SCI micelles and the skin aqueous pores. J Cosmet Sci. 2007; 58(3):229–244. [PubMed: 17598025]
20. Ghosh S, Blankschtein D. The role of sodium dodecyl sulfate (SDS) micelles in inducing skin barrier perturbation in the presence of glycerol. Int J Cosmetic Sci. 2007; 30:73.
21. Moore P, Puvvada S, Blankschtein D. Challenging the surfactant monomer skin penetration model: Penetration of sodium dodecyl sulfate micelles into the epidermis. J Cosmet Sci. 2003; 54:29–46. [PubMed: 12644857]
22. Yim B, Okuno H, Nagata Y, Nishimura R, Maeda Y. Sonlysis of surfactants in aqueous solutions: an accumlation of solute in the interfacial region of the cavitation bubbles. Ultrason Sonochem. 2002; 9(4):209–213. [PubMed: 12219583]
23. Chang CH, Wang NHL, Franses EI. Adsorption dynamics of single and binary surfactants at the air/water interface. Colloid Surface. 1992; 62(4):321–332.
24. Chang CH, Franses EI. Adsorption dynamics of surfactants at the air/water interface: a critical review of mathematical models, data, and mechanisms. Colloid Surface A. 1995; 100:1–45.
25. Kay RL, Lee KS. Micelle molecular parameters from surfactant ionic mobilities. J Phys Chem. 1986; 90(21):5266–5271.

26. Kameyama K, Takagi T. Micellar properties of octylglucosides in aqueous solutions. J Colloid Interf Sci. 1990; 137(1):1–10.
27. Tsochatzidis N, Guiraud P, Wilhelm A, Delmas H. Determination of velocity, size and concentration of ultrasonic cavitation bubbles by the phase-Doppler technique. Chem Eng Sci. 2001; 56(5):1831–1840.
28. Price GJ, Ashokkumar M, Grieser F. Sonoluminescence emission from aqueous solutions of organic monomers. J Phys Chem B. 2003; 107(50):14124–14129.
29. Segebarth N, Eulaerts O, Reisse J, Crum LA, Matula T. Correlation between acoustic cavitation noise, bubble population, and sonochemistry. J Phys Chem B. 2002; 106(35):9180–9190.
30. Skarbek-Borowska S, Becker BM, Lovgren K, Bates A, Minugh PA. Brief Focal Ultrasound With Topical Anesthetic Decreases the Pain of Intravenous Placement in Children. Pediatr Emerg Care. 2006; 22(5):339–345. [PubMed: 16714961]
31. Ashokkumar M, Hodnett M, Zeqiri B, Grieser F, Price GJ. Acoustic emission spectra from 515 kHz cavitation in aqueous solutions containing surface-active solutes. J Am Chem Soc. 2007; 129(8):2250–2258. [PubMed: 17279753]
32. Price GJ, Ashokkumar M, Hodnett M, Zeqiri B, Grieser F. Acoustic Emission from cavitating solutions: implications for the mechanisms of sonochemical reactions. J Phys Chem B. 2005; 109(38):17799–17801. [PubMed: 16853282]

Figure 1.
Skin sample treated with 4 mM octyl glucoside and 20 kHz LFS for 10 minutes. Regions stained by allura red are LTRs and unstained regions are non-LTRs.

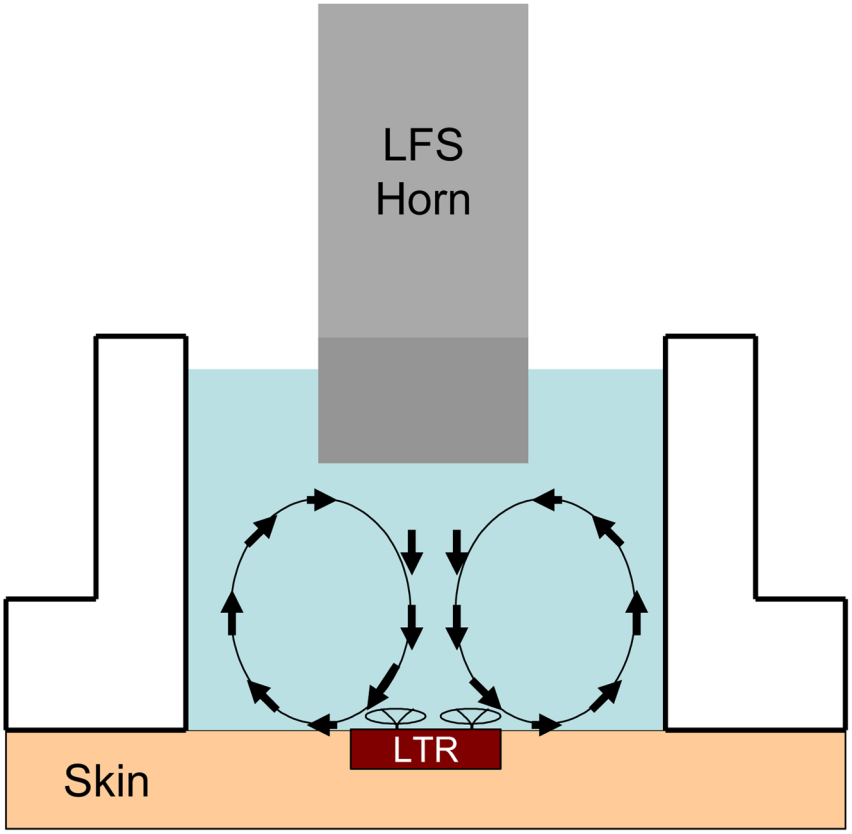

Figure 2.
Illustration of the physical mechanisms occurring during LFS treatment of skin. The top chamber of a Franz diffusion cell is shown in the illustration. Arrows represent an enhancement in stirring induced by acoustic streaming, with microjet collapse occurring above the LTR.

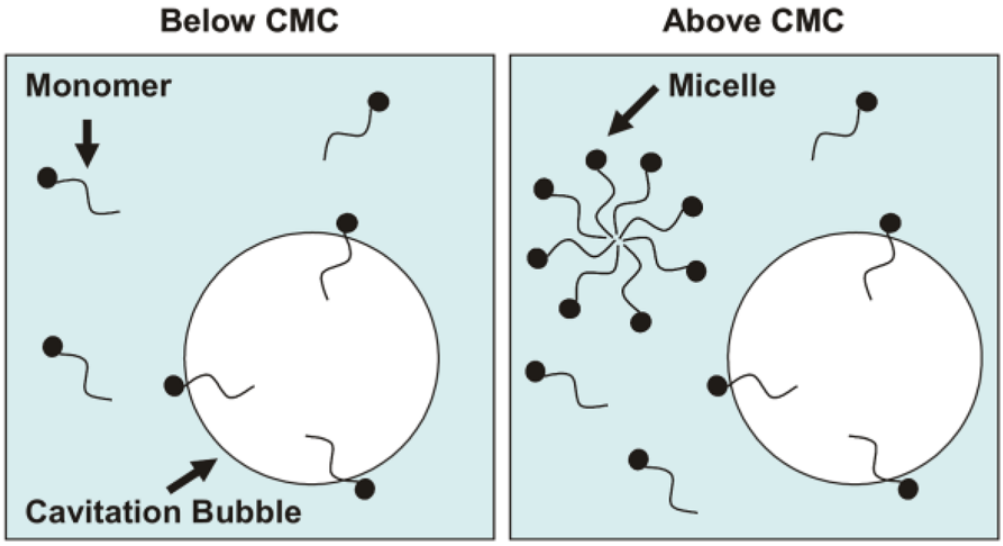

Figure 3.
Schematic illustration of amphiphilic monomers adsorbing to an acoustic cavitation bubble. Note that only the monomers can adsorb to cavitation bubbles and, therefore, the adsorbed monomer concentration is constant above the CMC.

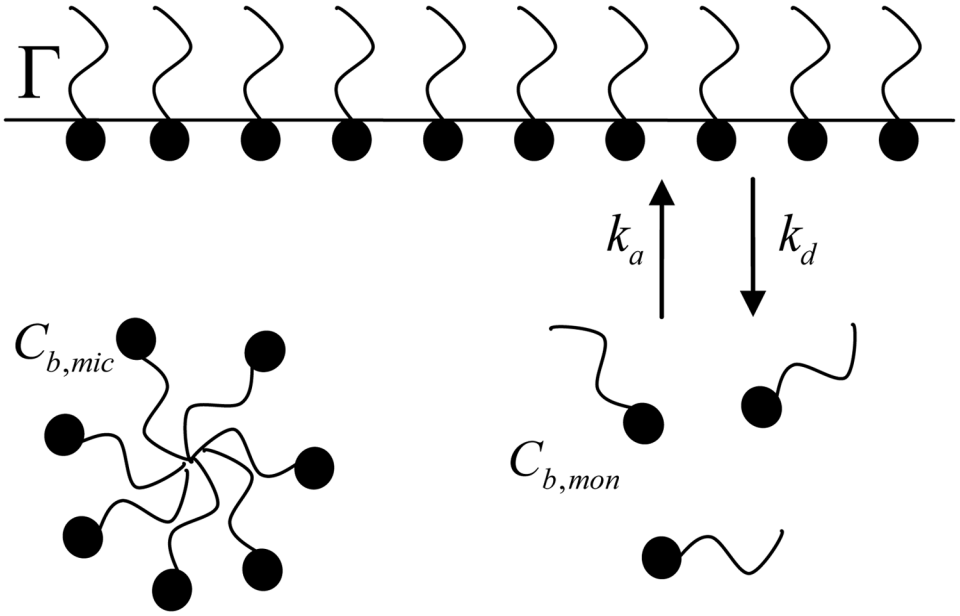

Figure 4.
Surfactant adsorption model utilized. Only monomers can adsorb to, and desorb from, the gas/water cavitation bubble interface. Monomers and micelles are assumed to be at equilibrium.

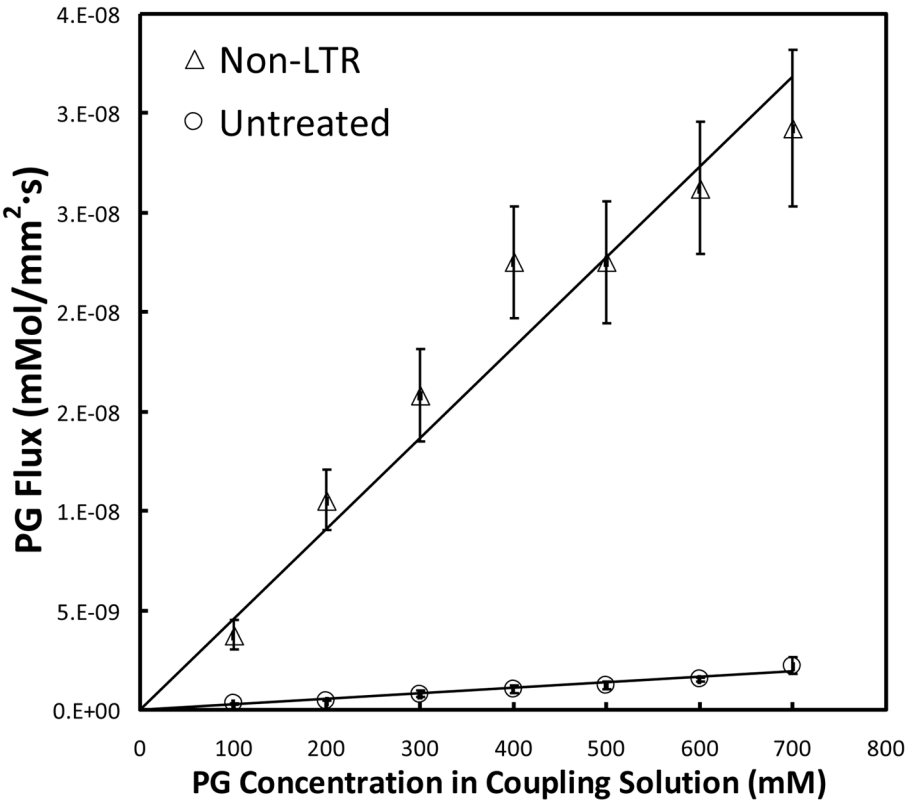

Figure 5.

Flux of PG into untreated skin and the non-LTRs of skin during LFS treatment as a function of OG concentration in bulk solution. The corresponding mass-transfer coefficients derived from the slopes of this data are reported in Table 5-1.

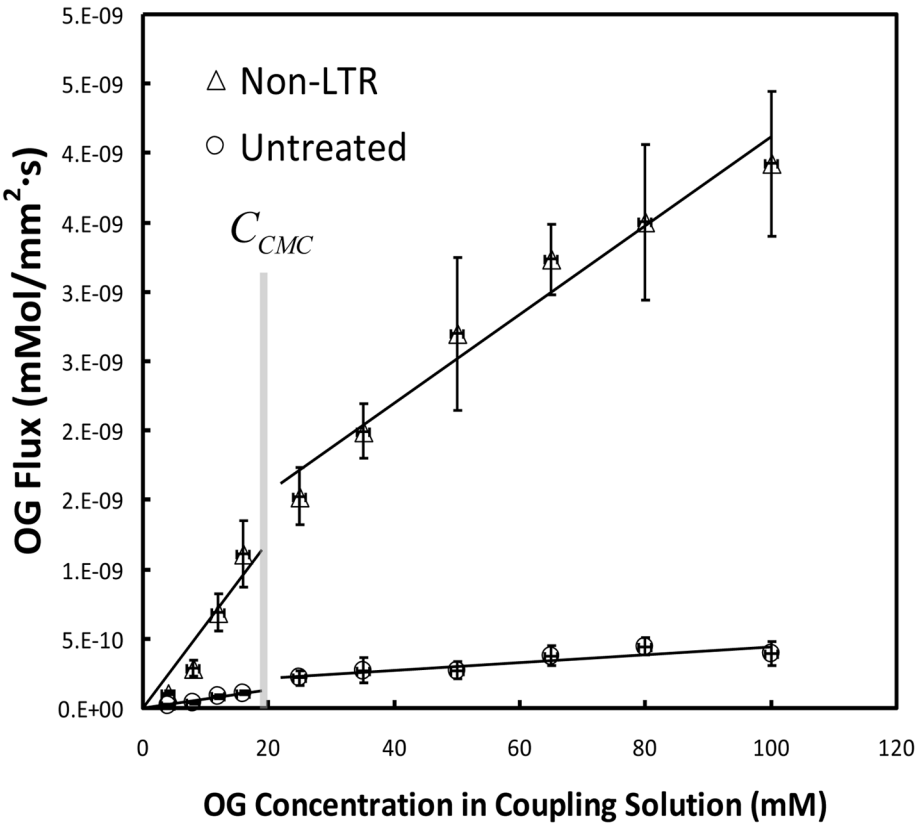

Figure 6.

Flux of OG into untreated skin and the non-LTRs of skin during LFS treatment as a function of PG concentration in bulk solution. The corresponding mass-transfer coefficients derived from the slopes of this data are reported in Table 5-1.

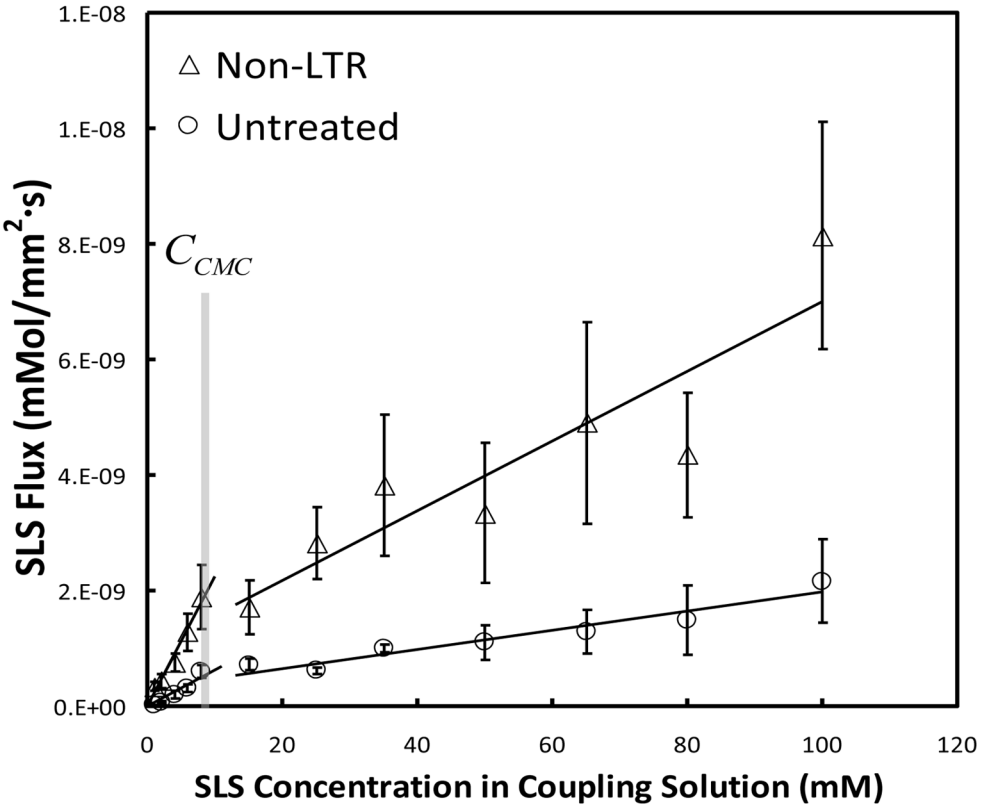

Figure 7.
Flux of SLS into untreated skin and the non-LTRs of skin during LFS treatment as a function of SLS concentration in bulk solution. The corresponding mass-transfer coefficients derived from the slopes of this data are reported in Table 1.

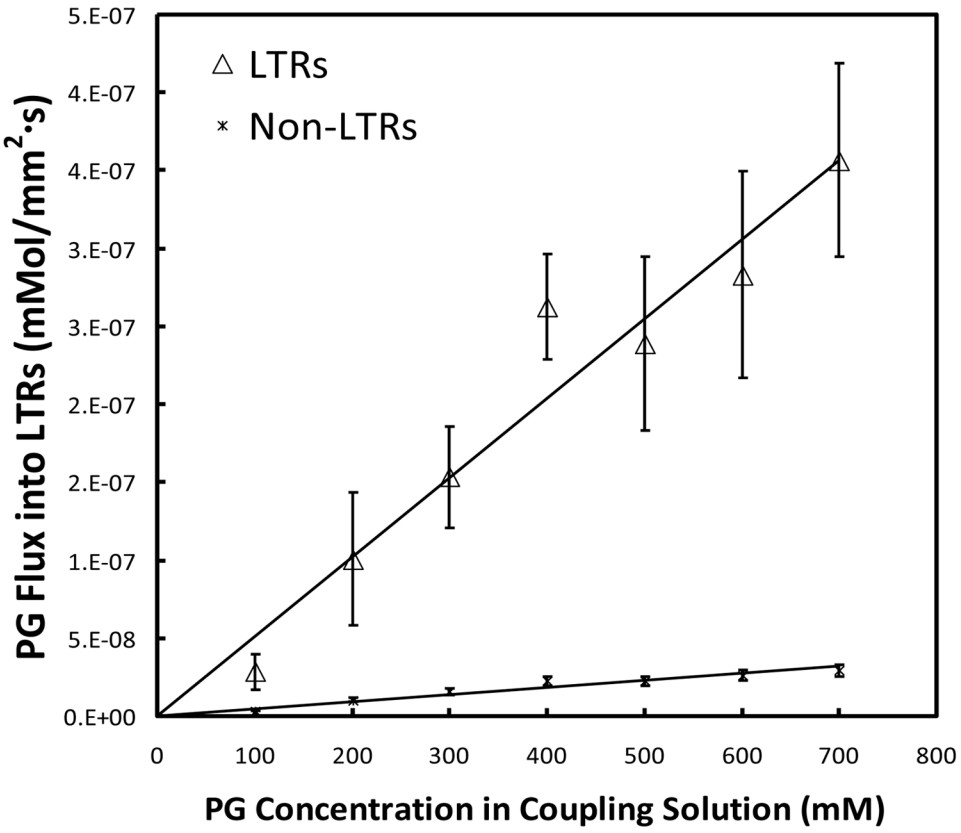

Figure 8.
Flux of PG into the LTRs of skin during LFS treatment as a function of PG concentration in the LFS coupling solution. The flux of PG into non-LTRs is shown for comparison.

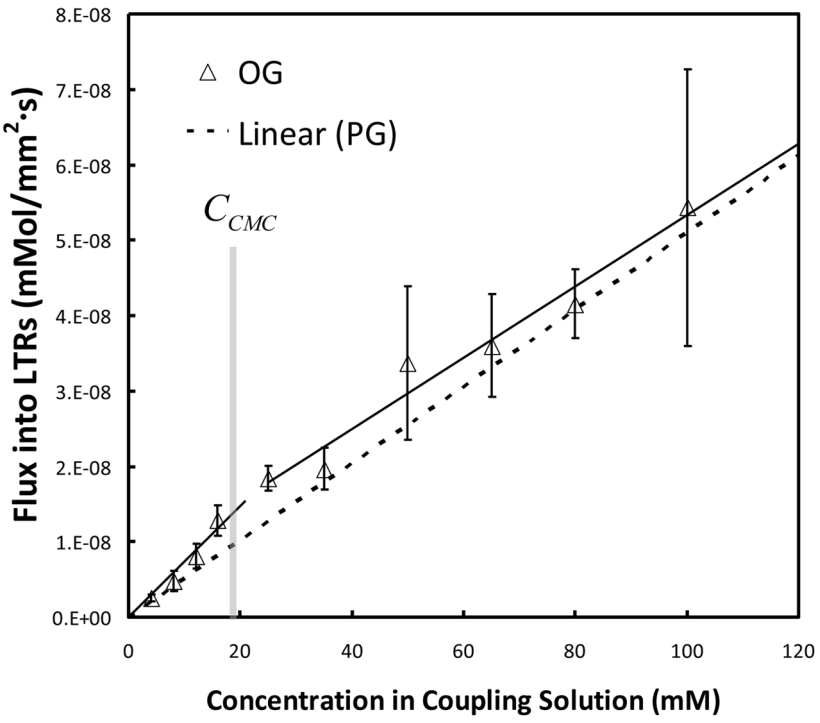

Figure 9.

Flux of OG into the LTRs of skin during LFS treatment as a function of OG concentration in the LFS coupling solution. The dashed line corresponds to the flux of PG, and is included for comparison purposes.

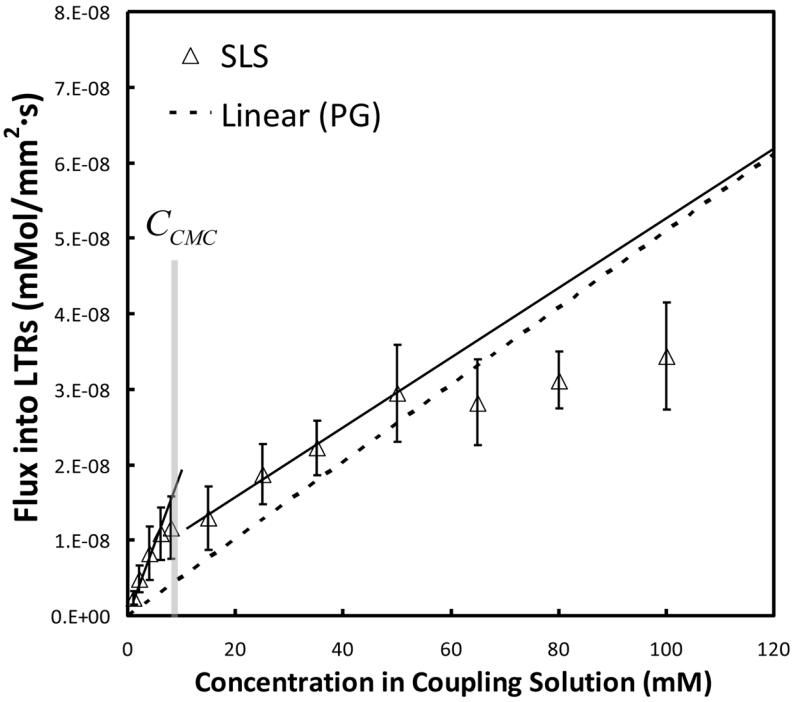

Figure 10.

Flux of SLS into the LTRs of skin during LFS treatment as a function of SLS concentration in the LFS coupling solution. The dashed line corresponds to the flux of PG, and is included for comparison purposes.

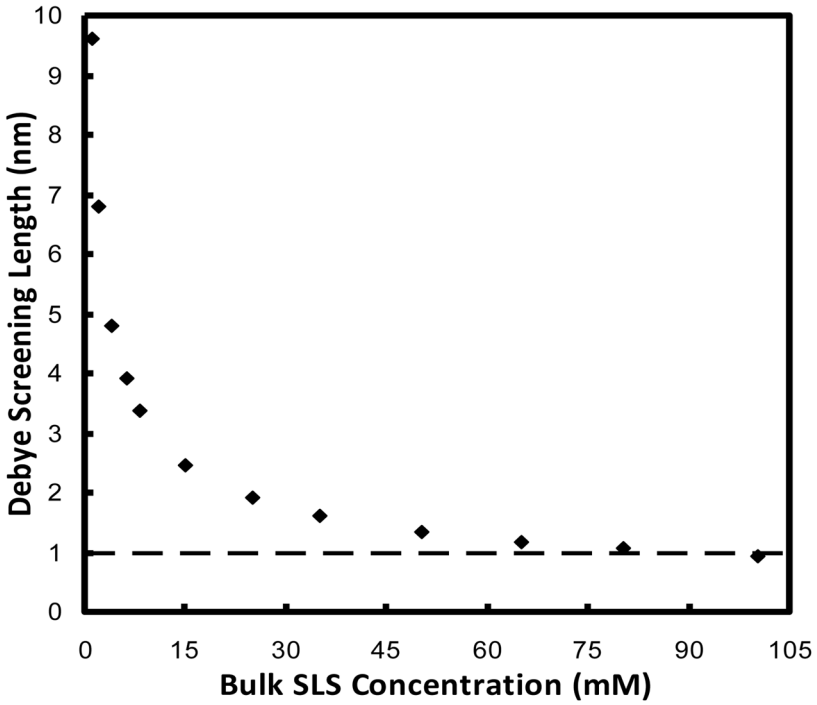

Figure 11.
Debye screening length as a function of SLS concentration, assuming complete dissociation.

Table 1

Mass-transfer coefficients of PG, OG, and SLS into untreated skin and the non-LTRs of skin during LFS treatment. Values were calculated from the slopes of the linear regressions shown in Figure 5–7, with the corresponding r^2 values reported.

CPE	Untreated Skin				Non-LTRs			
	$k_{m,mon}$	r^2	$k_{m,mic}$	r^2	$k'_{m,mon}$	r^2	$k'_{m,mic}$	r^2
PG	$2.7 \cdot 10^{-9}$ *m/s*	0.95	no CMC		$4.6 \cdot 10^{-8}$ *m/s*	0.93	no CMC	
OG	$6.5 \cdot 10^{-9}$ *m/s*	0.93	$2.8 \cdot 10^{-9}$ *m/s*	0.80	$6.0 \cdot 10^{-8}$ *m/s*	0.87	$3.2 \cdot 10^{-8}$ *m/s*	0.96
SLS	$6.3 \cdot 10^{-8}$ *m/s*	0.90	$1.7 \cdot 10^{-8}$ *m/s*	0.93	$2.2 \cdot 10^{-7}$ *m/s*	0.97	$6.0 \cdot 10^{-8}$ *m/s*	0.82

Table 2

Slopes of the permeant flux vs. bulk coupling medium concentration curves, both below and above the CMC of the tested CPEs

Species	$\dot{n}_{cav}$ (v_{cav} + $A_{cav}K_H$ (slope below CMC)		$\dot{n}_{cav}$ ·v_{cav} (slope above CMC)	
	value	r^2	value	r^2
PG	no CMC		$5.1 \cdot 10^{-7}$ *m*/*s*	0.94
OG	$7.3 \cdot 10^{-7}$ *m*/*s*	0.95	$4.7 \cdot 10^{-7}$ *m*/*s*	0.97
SLS	$1.9 \cdot 10^{-6}$ *m*/*s*	0.95	$4.6 \cdot 10^{-7}$ *m*/*s* (from 8–50 mM)	0.99